Mechanical Forces Guiding *Staphylococcus aureus* Cellular Invasion

Valeria Prystopiuk,[†] Cécile Feuillie,[†] Philippe Herman-Bausier,[†] Felipe Viela,[†] David Alsteens,[†] Giampiero Pietrocola,[‡] Pietro Speziale,*[‡,§] and Yves F. Dufrêne*[†,‖]

[†]Institute of Life Sciences, Université catholique de Louvain, Croix du Sud, 4-5, bte L7.07.06, B-1348 Louvain-la-Neuve, Belgium
[‡]Department of Molecular Medicine, Unit of Biochemistry, and [§]Department of Industrial and Information Engineering, University of Pavia, Viale Taramelli 3/b, 27100 Pavia, Italy
[‖]Walloon Excellence in Life Sciences and Biotechnology (WELBIO), 4000 Liège, Belgium

S *Supporting Information*

ABSTRACT: *Staphylococcus aureus* can invade various types of mammalian cells, thereby enabling it to evade host immune defenses and antibiotics. The current model for cellular invasion involves the interaction between the bacterial cell surface located fibronectin (Fn)-binding proteins (FnBPA and FnBPB) and the $\alpha 5\beta 1$ integrin in the host cell membrane. While it is believed that the extracellular matrix protein Fn serves as a bridging molecule between FnBPs and integrins, the fundamental forces involved are not known. Using single-cell and single-molecule experiments, we unravel the molecular forces guiding *S. aureus* cellular invasion, focusing on the prototypical three-component FnBPA–Fn–integrin interaction. We show that FnBPA mediates bacterial adhesion to soluble Fn *via* strong forces (~1500 pN), consistent with a high-affinity tandem β-zipper, and that the FnBPA–Fn complex further binds to immobilized $\alpha 5\beta 1$ integrins with a strength much higher than that of the classical Fn–integrin bond (~100 pN). The high mechanical stability of the Fn bridge favors an invasion model in which Fn binding by FnBPA leads to the exposure of cryptic integrin-binding sites *via* allosteric activation, which in turn engage in a strong interaction with integrins. This activation mechanism emphasizes the importance of protein mechanobiology in regulating bacterial–host adhesion. We also find that Fn-dependent adhesion between *S. aureus* and endothelial cells strengthens with time, suggesting that internalization occurs within a few minutes. Collectively, our results provide a molecular foundation for the ability of FnBPA to trigger host cell invasion by *S. aureus* and offer promising prospects for the development of therapeutic approaches against intracellular pathogens.

KEYWORDS: *mechanomicrobiology, mechanical forces, Staphylococcus aureus, invasion, host cells, atomic force microscopy*
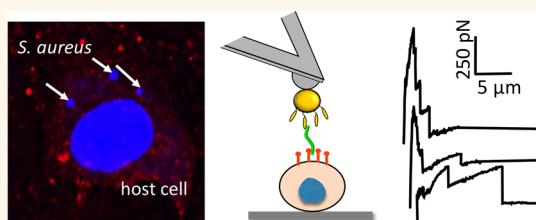
Staphylococcus aureus has long been considered as an extracellular bacterial pathogen, but it is now widely accepted that it can invade a variety of nonprofessional phagocytes such as endothelial cells,[1,2] epithelial cells,[3–5] and osteoblasts.[6,7] Internalized staphylococci may represent a reservoir that protects the bacteria from host immune defenses as well as from antibiotics. Invasive infection by *S. aureus* frequently involves bacterial seeding from the bloodstream to other body tissues, a process which requires circulating bacteria and vascular endothelial cells. *S. aureus* expresses a repertoire of surface-associated adhesion proteins (adhesins) that mediate either direct or indirect interaction with extracellular matrix (ECM) and endothelial cell surface components.[8] Direct interaction occurs when the adhesins recognize endothelial compounds, as observed for the binding of *S. aureus* protein A to the endothelial cell receptor gC1qR/p33.[9] Indirect interaction is when adhesins bind to plasma proteins immobilized on damaged endothelial cells or bound to specific cell receptors. An example of this is the von Willebrand factor

(vWF)-binding protein, which mediates bacterial attachment to endothelial cells under shear.[10] Likewise, fibrinogen (Fg) acts as a bridge between *S. aureus* protein ClfA and integrin $\alpha 5\beta 3$ expressed by sheared endothelial cells.[11]

During the early stage of invasion, *S. aureus* attaches to endothelial cells *via* the binding of fibronectin (Fn)-binding proteins (FnBPA and FnBPB) to $\alpha 5\beta 1$ integrins on the host cell surface.[12] This interaction involves the extracellular matrix protein Fn, which acts as a bridging molecule between FnBPs and integrins (Figure 1a).[5,13,14] Soluble Fn is a dimeric glycoprotein with distinct domains, each composed of multiples modules of <100 amino acids, named type I, II, and III repeats (Figure 1a). Full-length FnBPA harbors 11 Fn-binding repeats that specifically interact with four sequential modules of the N-terminal FI domain *via* a tandem β-zipper.[15] Of the 11 Fn-
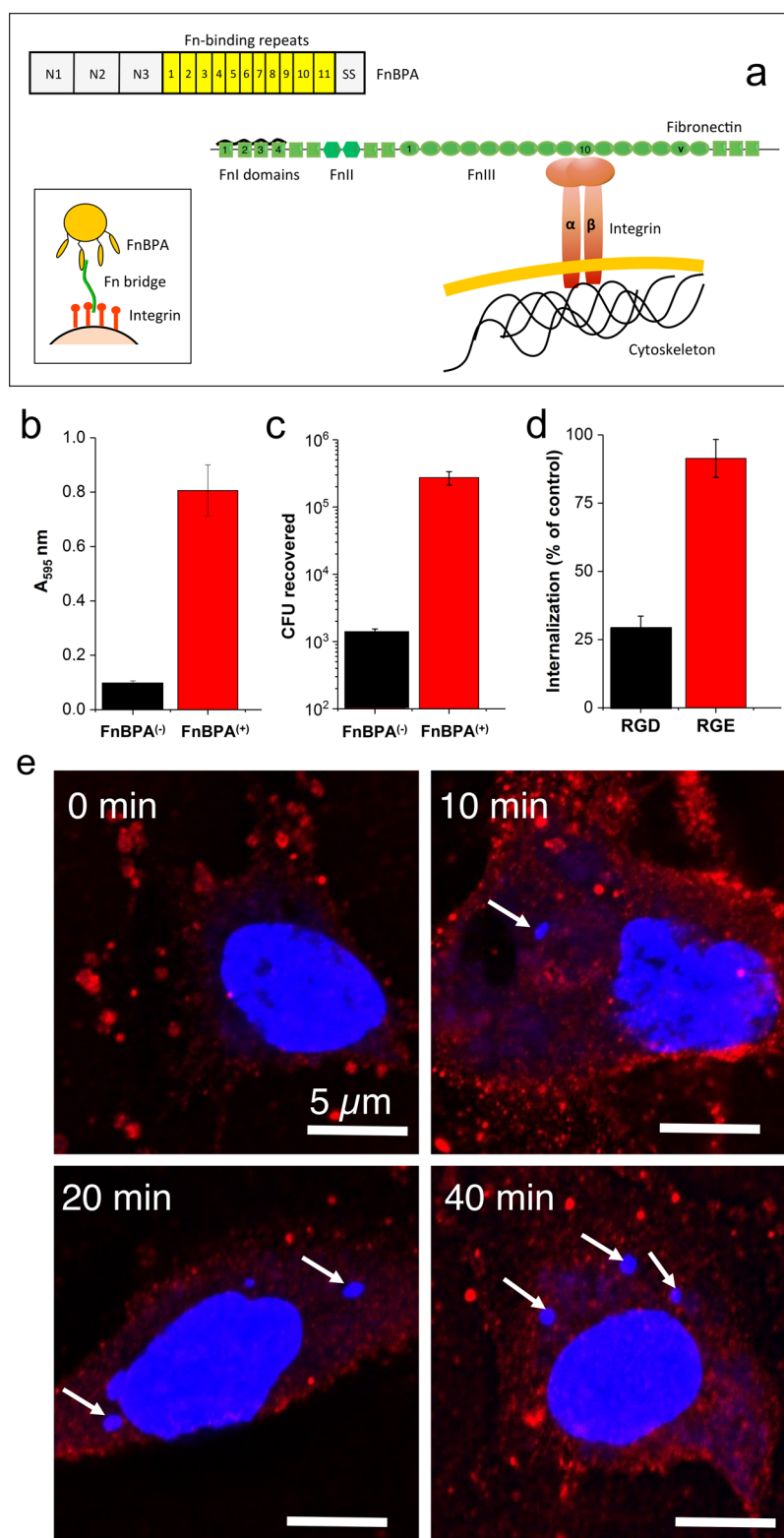
Figure 1. Role of FnBPA in cellular invasion. (a) Mechanism of FnBP-dependent cell invasion by *S. aureus*. The main invasion pathway of *S. aureus* involves interaction of the Fn-binding repeats of FnBPA with type I Fn modules *via* a tandem β-zipper structure. This triggers a conformational change in Fn, resulting in the exposure of the cryptic integrin-binding site in the tenth FnIII module, which in turn engages in a high-affinity interaction with the $\alpha 5\beta 1$ integrin found in the membrane of mammalian cells. (b) Adherence of bacteria to immobilized Fn. Microtiter wells coated with Fn were incubated with *S. aureus* FnBPA$^{(+)}$ and FnBPA$^{(-)}$ bacteria. After fixation with formaldehyde and staining with crystal violet, adhering cells were quantified by measuring the absorbance at 595 nm in an ELISA plate reader. Means and standard deviation of results of two independent experiments, each performed in triplicate, are presented. (c) Invasion of endothelial cells by *S. aureus*. HUVEC monolayers were incubated with *S. aureus* FnBPA$^{(+)}$ and FnBPA$^{(-)}$ bacteria for 90 min. Means and standard deviation of results of two independent experiments, each performed in triplicate, are presented. (d) Inhibitory effect of an RGD-containing peptide on cellular invasion. HUVEC were incubated for 10 min with 20 mM of the RGD or RGE peptides prior the addition of *S. aureus* FnBPA$^{(+)}$ bacteria.

Figure 1. continued

Invasion levels are expressed as percentages of invasion observed in the absence of peptides (control; 3×10^5 colony-forming units, CFU). Means and standard deviation of results of two independent experiments, each performed in triplicate, are presented. (e) Confocal microscopy imaging of internalized *S. aureus* bacteria. HUVEC monolayers were incubated with *S. aureus* FnBPA$^{(+)}$ bacteria for 10, 20, and 40 min. Samples were then stained with DAPI (blue) to label the cell nucleus and *S. aureus* bacteria and with anti-integrin $\alpha 5 \beta 1$ antibodies (red) to label host cell integrins. The small blue dots (white arrows) indicate that *S. aureus* bacteria are already internalized after 10 min.
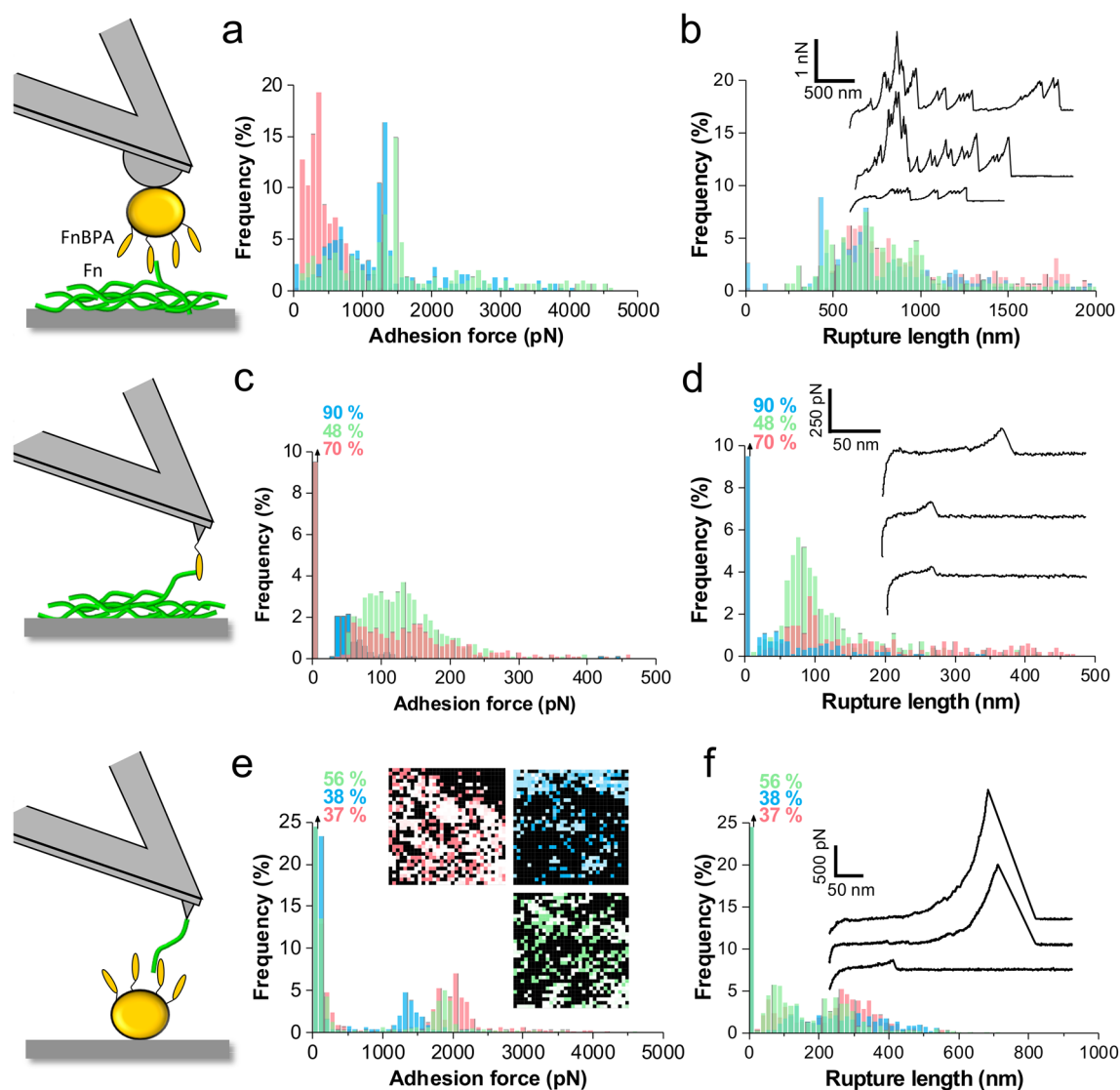
Figure 2. Strength of the FnBPA−Fn tandem β-zipper. (a,b) Maximum adhesion force and rupture length histograms with representative force profiles obtained by recording force−distance curves in HEPES buffer between *S. aureus* FnBPA$^{(+)}$ cells and Fn immobilized on solid substrates. Data from a total of 923 curves from three different cells are shown. (c,d) Force data obtained between AFM tips bearing recombinant FnBPA Fn-binding repeats and Fn substrates (3072 curves from three tips). (e,f) Force data obtained between AFM tips bearing Fn and *S. aureus* FnBPA$^{(+)}$ cells (3072 curves from three cells). The insets in (e) are adhesion maps documenting the localization of FnBPAs (force scale = 2000 pN, image size = 500 nm). Histograms were obtained by calculating, for each curve, the force of the strongest adhesive event (a,c,e) and the distance of the last rupture event (b,d,f). Percentages shown represent the proportion of nonadhesive events.

binding repeats, six exhibit high-affinity binding of Fn,[16] and a single high-affinity repeat is sufficient for $\alpha 5 \beta 1$ integrin-dependent invasion of endothelial cells by *S. aureus*.[14]

Despite the biological importance of FnBP-mediated cellular invasion, the molecular interactions involved are poorly understood. Specifically, the mechanical stability of the Fn bridge between FnBPA and the $\alpha 5 \beta 1$ integrin has never been studied. Here, we address this issue using single-molecule and single-cell atomic force microscopy (AFM) experiments.[17,18]

The results show that FnBPA binds to Fn *via* a β-zipper structure, and that this complex in turn enhances bacterial attachment to host cells by forming a mechanically strong bridge with the $\alpha 5 \beta 1$ integrin. The Fn bridge can withstand much stronger forces than the classical Fn−$\alpha 5 \beta 1$ integrin interaction. Intercellular adhesion dramatically strengthens with time, suggesting that bacteria are internalized within a few minutes. This work represents an important step forward in the development of innovative techniques for studying the

molecular basis of *S. aureus*—host interactions and for the design of antistaphylococcal agents, which may find applications in various fields including molecular and cellular microbiology, pathogenesis and drug discovery.

RESULTS AND DISCUSSION

FnBPA-Dependent Cellular Invasion. To selectively study the role of FnBPA in adhesion and invasion, full-length FnBPA was expressed from a plasmid in *S. aureus* strain SH1000 defective in clumping factors (Clfs) A and B and in FnBPA and B (hereafter *S. aureus* FnBPA$^{(+)}$ cells). We validated the expression of fully functional adhesins on the bacterial surface by comparing the ability of *S. aureus* FnBPA$^{(+)}$ and FnBPA$^{(-)}$ cells to attach to Fn-coated microtiter wells. FnBPA$^{(+)}$ bacteria largely adhered to Fn, whereas those lacking the adhesin did to a much lower extent (Figure 1b). Furthermore, using a standard invasion assay of human umbilical vein endothelial cells (HUVEC) (Figure 1c), FnBPA$^{(+)}$ cells, but not FnBPA$^{(-)}$ ones, were found to massively invade endothelial cell monolayers. FnBPA$^{(-)}$ cells showed some residual levels of invasion, which suggests that other minor invasion pathways are operational in the internalization process. To further test the specificity of invasion, integrins were blocked by incubating endothelial cells with the tripeptide arginine—glycine—aspartic acid (RGD). This peptide, found in numerous proteins including Fn, specifically binds to integrin receptors.[19,20] Whereas the control peptide RGE had no inhibitory effect, the RGD peptide strongly reduced the level of invasion by *S. aureus* FnBPA$^{(+)}$ cells (Figure 1d). This confirms that the specific interaction of $\alpha5\beta1$ integrins with Fn is required for efficient invasion of host cells by *S. aureus* FnBPA$^{(+)}$ cells.[21]

We tracked the dynamics of *S. aureus* invasion using confocal microscopy. Confluent HUVEC cultured for 48 h were incubated with *S. aureus* FnBPA$^{(+)}$ bacterial cells up to 40 min and then further fixed. Using three-dimensional imaging analysis, we could identify *S. aureus* cells (blue labeling indicates DNA from the HUVEC nucleus and from intracellular bacteria) inside HUVEC (red labeling indicates $\alpha5\beta1$ integrins), already after 10 min of incubation, thus confirming that invasion already took place (Figure 1e). Vertical and horizontal cross sections of infected cells (Figure S1) confirmed internalization of the bacteria. After 40 min of incubation, most endothelial cells were infected, in agreement with previously published data.[5,12,22]

Mechanical Strength of the FnBPA—Fn Tandem β-Zipper. The Fn-binding repeats of FnBPA align antiparallel with up to five FnI modules to form a tandem β-zipper.[23] While FnBP—Fn interactions have already been studied by AFM,[24−29] evidence for a mechanically strong β-zipper structure has never been reported. We therefore explored the interaction forces between FnBPA and Fn immobilized on solid substrates. *S. aureus* FnBPA$^{(+)}$ cells were attached on colloidal cantilevers,[30,31] allowing us to measure the forces between single bacteria and Fn-coated surfaces. Force—distance curves featured adhesion forces ranging from 50 up to 5000 pN, and with rupture lengths of 50—2000 nm (Figure 2a,b). Adhesion force profiles showed complex shapes with multiple peaks, indicating that multiple intermolecular bonds were probed. Interestingly, many cells showed a sharp maximum in their force distribution at 1387 ± 179 pN (mean ± SD from 254 adhesive curves), suggesting that FnBPA—Fn adhesion involves strong bonds.

To unambiguously capture the strength of single FnBPA—Fn bonds, we investigated the interaction between recombinant Fn-binding repeat regions of FnBPA and Fn substrates (Figure 2c,d). Single well-defined adhesion peaks of 120 ± 51 pN (mean ± SD; *n* = 873 adhesive curves) were observed, which lies in the range of values reported for FnBP—Fn interactions.[24,28] In particular, the strength of interaction between a synthetic peptide mimicking a single Fn-binding repeat and Fn has recently been shown to be on the order of ∼100 pN.[29] Force experiments between Fn tips and FnBPA$^{(+)}$ cells (Figure 2e,f) yielded not only similar weak forces (∼100 pN) but also strong forces of ∼1500 pN (cell #1, 1931 ± 280 pN, from *n* = 365 adhesive force curves; cell #2, 1427 ± 289 pN, *n* = 209; cell #3, 1840 ± 263 pN, *n* = 216). Single-molecule mapping revealed that FnBPA localized heterogeneously on the bacterial cell surface (Figure 2e, inset), suggesting that, *in vivo*, the adhesin may engage in multivalent interactions to enhance bacterial adhesion.

We believe that the high forces observed on living bacteria are associated with the unusual β-sheet organization of the FnBPA—Fn tandem β-zipper, and weak forces involve single repeats not engaged in a zipper structure. The idea behind the tandem β-zipper is that, upon binding to the FnI modules, the intrinsically disordered Fn-binding repeats of FnBPA shift into an ordered structure by forming additional β-strands along triple peptide β-sheets in the Fn molecule. Why were strong forces never detected with recombinant FnBPA domains? The number of bonds probed in protein experiments might be smaller, as suggested by the lower frequency of binding. Another explanation is that when the repeats are attached randomly to a surface through multiple sites, without being properly oriented as in the bacterial cell wall, conformational changes needed for the β-zipper complex will be hindered. Because the β-zipper shows a mechanical stability (∼1500 pN) in the range of that of covalent bonds,[32] one may argue that the S—Au bonds might break during the measurements. In such a case, however, we would expect the adhesins to be blocked and/or deactivated, which was never observed even after recording hundreds of force curves. The β-zipper features force signatures that differ from classical AFM unzipping experiments, where the sequential unbinding of multiple bonds leads to force plateaus.[33,34] These observations favor a mechanism where all bonds of the β-sheet zipper rupture simultaneously, rather than sequentially, thus explaining the high mechanical stability of the complex. Such a behavior implies that the bonds are pulled in a shear geometry and rupture cooperatively, like when stretching dsDNA at both 3′ ends.[35] By contrast, in a zipper geometry, such as when pulling dsDNA on the 3′ and 5′ ends,[35] multiple bonds rupture one-by-one along the applied force.

Probing FnBPA$^{(+)}$ cells with Fn tips resulted in protein extensions varying from ∼25 to ∼500 nm (Figure 2f), with the most frequently observed values being 309 ± 86 nm (*n* = 1074; three cells). Fully extended FnBPA proteins (948 amino acids) should give polypeptide chains of ∼350 nm,[36] suggesting that the high forces were sufficient to fully unfold the adhesins. When Fn was attached on a substrate, longer extensions were seen (Figure 2b), up to 2000 nm, implying that Fn molecules were unfolded, as well. In line with this, some force profiles showed periodic peaks documenting the unfolding of the multiple Fn repeats.

Binding Forces between FnBPA and Fn in the Extracellular Matrix. We then studied FnBPA—Fn inter-
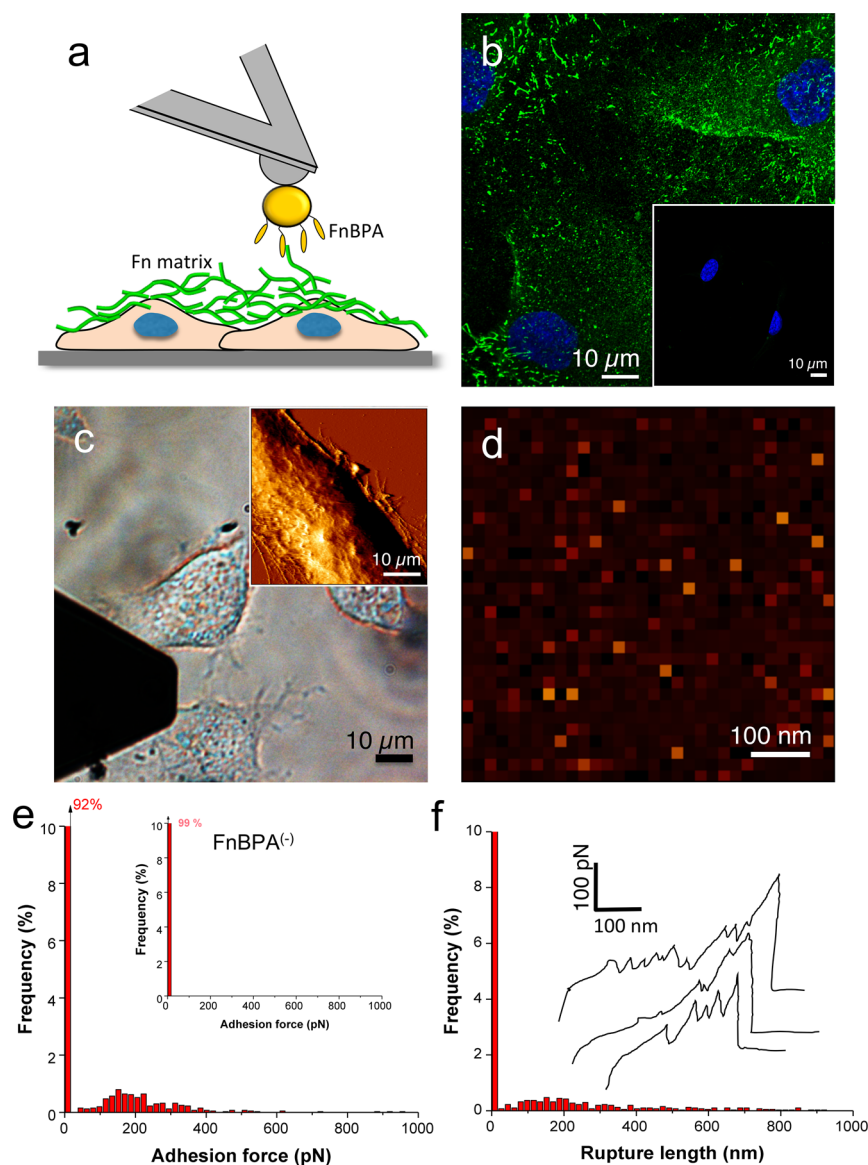
Figure 3. Forces between FnBPA and the extracellular matrix. (a) To study the interaction between FnBPA and Fn in the ECM, we measured the forces between FnBPA$^{(+)}$ bacterial probes and HUVEC monolayers spread on glass for 48 h. (b) Confocal microscopy image after staining with DAPI and anti-Fn antibody, documenting the production of large amounts of Fn (Fn is in green, nuclei in blue). The inset shows a control experiment in which primary anti-Fn antibody was missing. (c) Optical (DIC) microscopy image and AFM image (inset) revealing that the cells were well-spread on the substrate. (d−f) Adhesion force map (force scale = 400 pN), adhesion force histogram, rupture length histogram, and representative force profiles obtained by recording force−distance curves in HEPES between *S. aureus* FnBPA$^{(+)}$ bacteria and confluent endothelial cells. Histograms in (e) and (f) are from a total of 4027 curves from five independent cell pairs. They were obtained by calculating, for each curve, the force of the strongest adhesive event (e) and the distance of the last rupture event (f). Percentage shown represents the proportion of nonadhesive events.

actions between *S. aureus* bacteria and Fn in the ECM of endothelial cells. HUVEC were allowed to spread on glass Petri dishes for 48 h to favor the production of ECM proteins (Figure 3a). Fluorescence imaging of confluent cells revealed that Fn was produced in large amounts (Figure 3b), while differential interference contrast (DIC) microscopy and AFM images confirmed that the cells were well-spread on the substrate (Figure 3c). Figure 3d−f shows the adhesion force map and histogram, rupture length histogram, and typical force curves collected between single FnBPA$^{(+)}$ bacteria and endothelial cells. Multiple adhesion peaks of 225 ± 127 pN magnitude (mean ± SD; *n* = 298 adhesive curves from five cell pairs) and 100−1000 nm rupture lengths were randomly

detected across the endothelial cell surface. These events were abolished with FnBPA$^{(−)}$ cells (see inset in Figure 3e), meaning they mainly originate from specific FnBPA−Fn bonds.

Our results show that the strength of FnBPA−Fn bonds is higher on soluble Fn (∼1500 pN) than on Fn from the ECM of endothelial cells (∼200 pN). However, these two sets of experiments should not be quantitatively compared because HUVEC produce Fn, which structurally differs from soluble Fn. While soluble Fn forms dimers that are in a globular compact state, Fn in the ECM is mostly present in a fibrillar, extended state created by tension generated through the binding to cell surface receptors.[37,38] The involvement of receptors like integrins in the promotion of Fn fibrillogenesis explains why
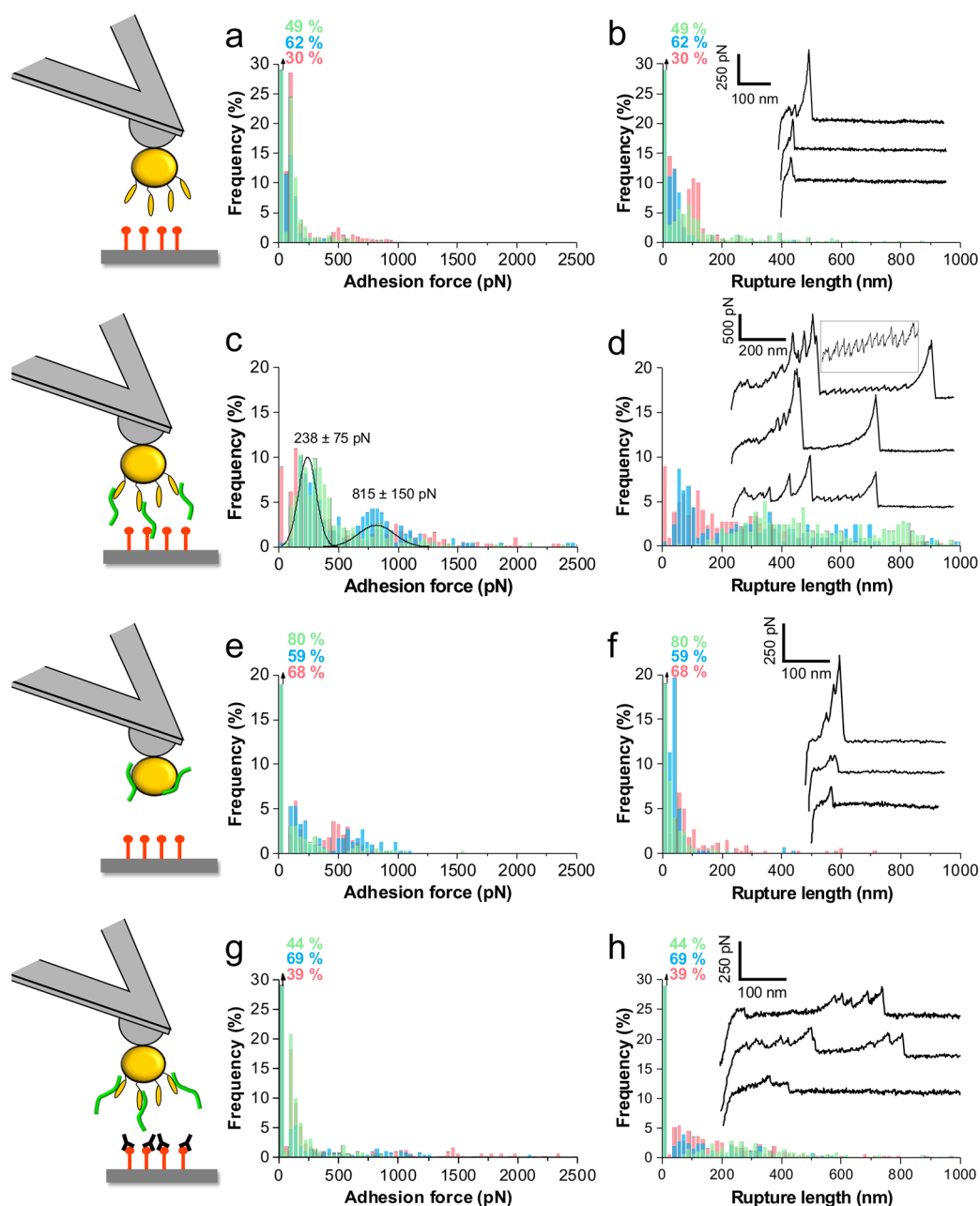
Figure 4. Mechanical stability of the Fn bridge between FnBPA and the $\alpha 5\beta 1$ integrin. (a,b) Adhesion force and rupture length histograms with representative force profiles obtained by recording force−distance curves in HEPES between *S. aureus* FnBPA[(+)] cells and $\alpha 5\beta 1$ integrins immobilized on solid substrates. Data from a total of 1244 curves from three different cells are shown. (c,d) Force data obtained between *S. aureus* FnBPA[(+)] cells pretreated with soluble Fn and integrin substrates (1171 curves from three cells). (e,f) Force data obtained between *S. aureus* FnBPA[(−)] cells pretreated with soluble Fn and integrin substrates (958 curves from three cells). (g,h) Force data obtained between Fn-saturated *S. aureus* FnBPA[(+)] cells and integrin substrates, following addition of anti-$\alpha 5\beta 1$ integrin antibodies (900 curves from three cells). Histograms were generated by considering, for every curve, the force and the distance of the last rupture event. Percentages shown represent the proportion of nonadhesive events.

this phenomenon is produced only by living cells in culture. In addition, fibrillar Fn also establishes a variety of interactions with other components of the extracellular matrix (collagens, heparin, *etc.*). So changes in the Fn structure (soluble *vs* fibrillar) may explain differences in the strength of the FnBPA−Fn interaction. *In vivo*, we expect that *S. aureus* will encounter both soluble and fibrillar Fn, enabling the formation of the β-zipper structure. Finally, it is possible that AFM will not detect the high-affinity tandem β-zipper interaction in the ECM due to the relatively weak anchoring strength of Fn to the cell matrix.

Under force, the Fn−matrix bond may rupture before the strong tandem β-zipper.

We note that extended force plateaus were never observed in the above experiments, thus pulling on FnBPA−Fn bonds did not lead to the extraction of lipid tethers from the cell membrane.[39,40] This suggests that when endothelial cells were spread on glass, direct contact of the bacteria with the membrane was hindered by the production of large amounts of ECM proteins (Figure 3a,b).
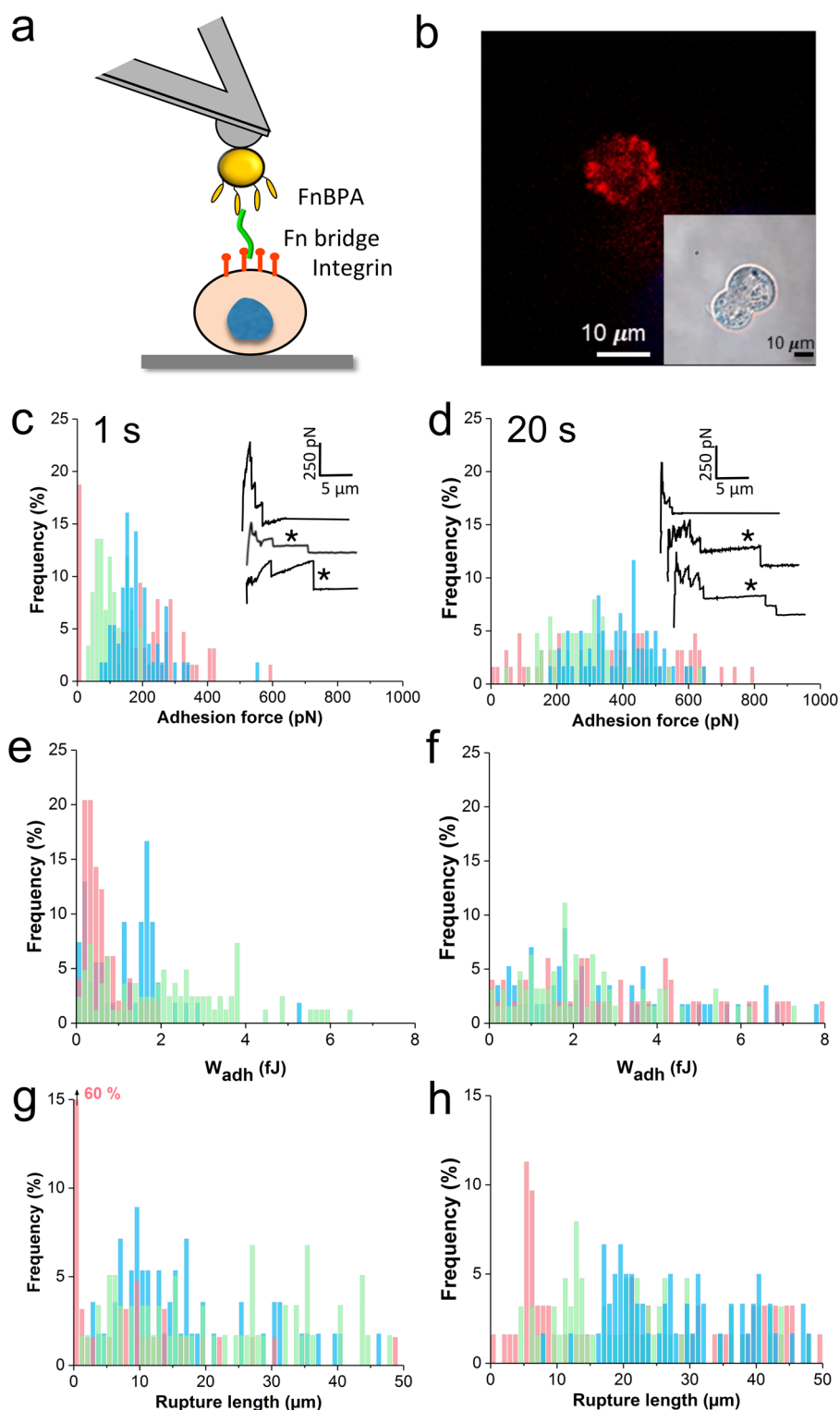
Figure 5. Fn-dependent adhesion forces between *S. aureus* and endothelial cells. (a) To promote the exposure of α5β1 integrins in the upper cell membrane, HUVEC were trypsinized to remove ECM proteins and immobilized on glass substrates coated with ConA lectins and then quickly analyzed. (b) Confocal microscopy image of an endothelial cell stained with anti-integrin α5β1 antibodies showing that integrins are exposed in the upper membrane and available for interaction (red color). The inset is an optical (DIC) image showing the round shape of the cell, as opposed to the flat shape of confluent cells. (c,e,g) Histograms showing the distributions of maximum adhesion forces, works of adhesion and rupture lengths, with typical force profiles, obtained in HEPES after 1 s of interaction between *S. aureus* FnBPA[(+)] bacteria and endothelial cells exposing integrins in their upper membrane. Data from a total of 192 curves from three different cell pairs are shown. (d,f,h) Force results obtained after increasing the interaction time from 1 to 20 s (192 curves from three cell pairs). Histograms were obtained by calculating, for each curve, the force of the strongest adhesive event and the distance of the last rupture event. Percentage shown represents the proportion of nonadhesive events.
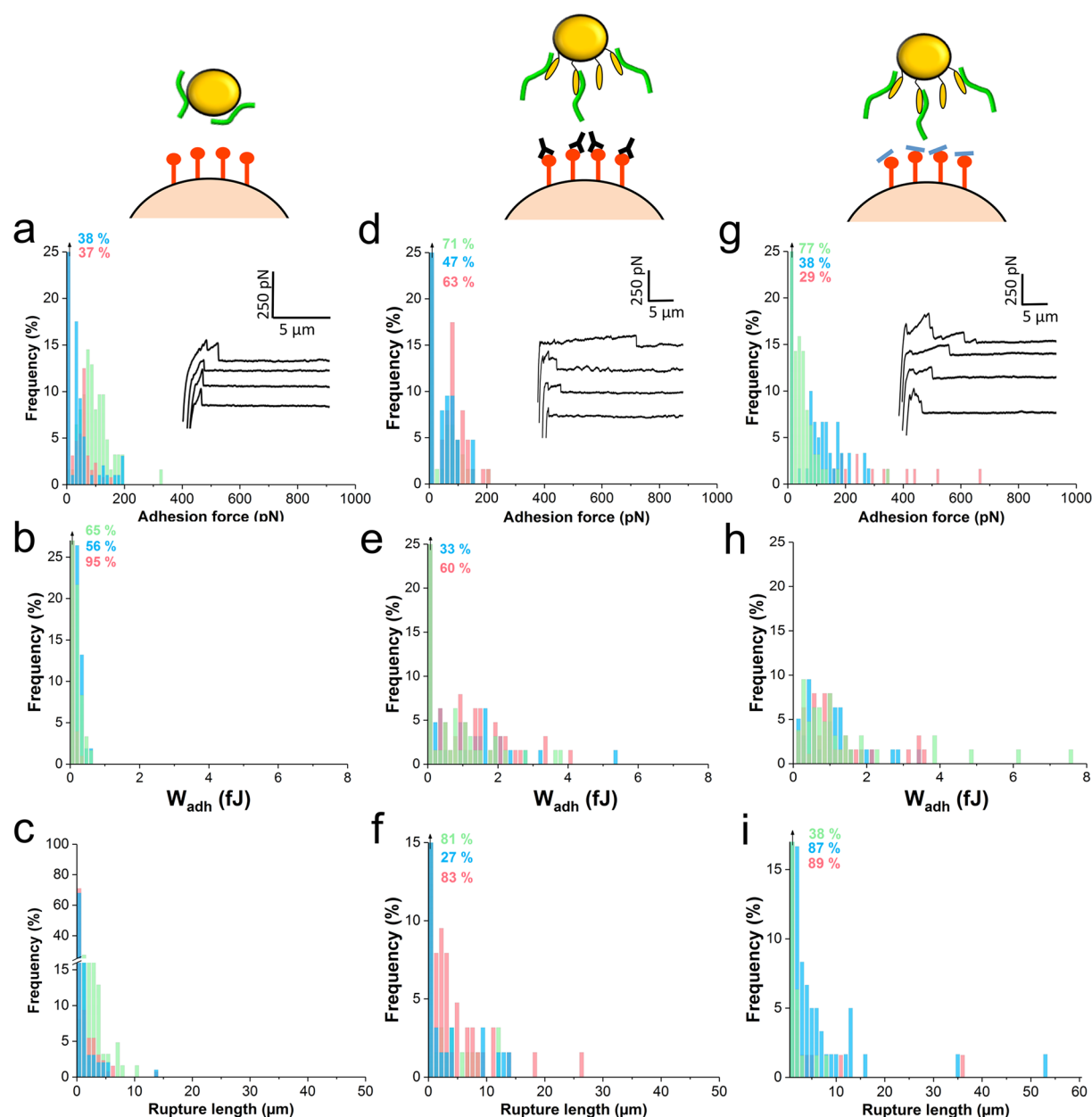
Figure 6. Control experiments showing that bacterial−host adhesion involves a Fn bridge. (a−c) Histograms showing the distribution of adhesion forces, works of adhesion, and rupture lengths, with typical force profiles, obtained in HEPES after 1 s of interaction between Fn-saturated *S. aureus* FnBPA[(−)] bacteria and endothelial cells exposing integrins in their upper membrane. The colors correspond to three different cell pairs. Force data between Fn-saturated *S. aureus* FnBPA[(+)] bacteria and endothelial cells, following addition of anti-α5β1 integrin antibodies (1/200 v/v) (d−f) or RGD peptides (0.1 mg mL^{−1}) (g−i). For each set of experiments, data from a total of 192 curves from three different cell pairs are shown. Percentages shown represent the proportion of nonadhesive events.

Fn Forms a Mechanically Strong Bridge between FnBPA and the α5β1 Integrin. To determine the mechanical stability of the Fn bridge between *S. aureus* FnBPAs and α5β1 integrins on host cells, we postulated that incubation of bacterial cells with soluble Fn should activate their interaction with integrins. We tested this idea by quantifying adhesion forces between FnBPA[(+)] cells pretreated with soluble Fn and α5β1 integrins immobilized on solid substrates. While most forces between native FnBPA[(+)] cells and immobilized integrins were weak (114 ± 45 pN; n = 594 adhesive curves from three cells; Figure 4a,b), incubating the bacteria with Fn dramatically increased the adhesion frequency, adhesion force, and rupture length (Figure 4c,d), thus demonstrating that soluble Fn

promotes bacterial adhesion to integrins. The distribution of adhesion forces showed two maxima at 238 ± 75 and 815 ± 150 pN (Gaussian fits; n = 1121 adhesive curves from three cells). Several observations led us to believe that the ∼800 pN force profiles represent the signature of the Fn-dependent bridging interaction between FnBPA and the α5β1 integrin. First, the specificity of binding was tested by using FnBPA[(−)] cells lacking the adhesin (Figure 4e,f) or by adding anti-integrin antibodies to the buffer (Figure 4g,h). Both the adhesion probability and adhesion force were substantially reduced, supporting the view that FnBPA and integrins are engaged in the interaction. Second, high force profiles often showed periodic peaks separated by 28 ± 5 nm (n = 130) (Figure 4d,
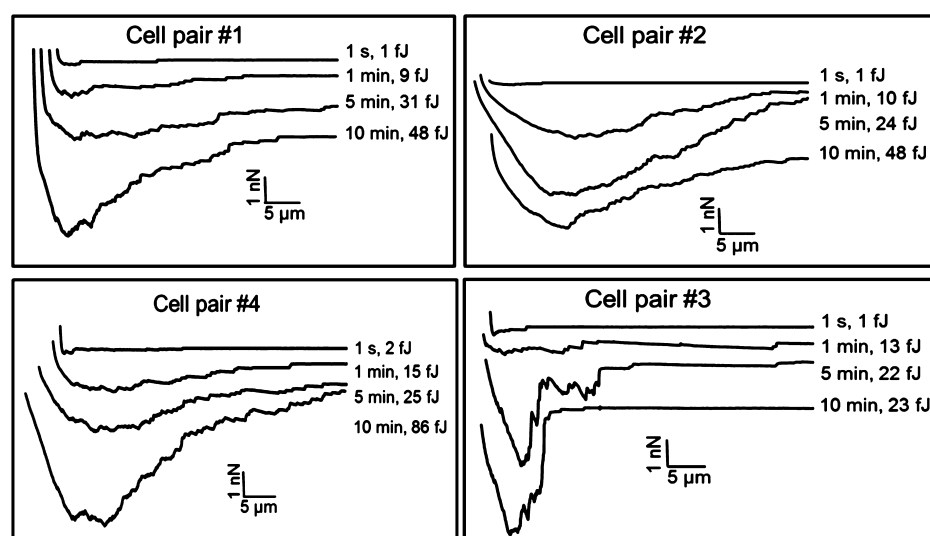
Figure 7. Bacterial−host adhesion strengthens with time. Sequences of force curves obtained between Fn-saturated *S. aureus* FnBPA[(+)] bacteria and endothelial cells after 1 s, 1 min, 5 min, and 10 min of interaction. Results from four different cell pairs are shown.

inset), which matches perfectly the unfolding of the multiple Fn repeats. Soluble dimeric Fn has more than 50 modules with the structural β-sheet motifs FnI, FnII, and FnIII. Specifically, FnIII domains have been shown to unfold with forces ranging from 80 to 200 pN, leading to an increase in contour length of 28 nm for each unfolded domain.[41] Third, unlike in control experiments, high forces featured very long ruptures (up to 1000 nm) with three distinct parts, that is, a first strong adhesion peak with rather high force (500−1000 pN) reflecting protein unfolding, a sawtooth pattern of low force (100 pN) due to Fn repeat unfolding, and then another strong adhesion peak (500−1000 pN) that may represent the detachment of integrins from the three-component complex. Under force, we expect that FnBPA will not detach from Fn given the high mechanical strength of the FnBPA−Fn β-zipper (∼1500 pN).

Two interesting questions are whether α5β1 integrins were still functional after immobilization, and how strong are single Fn−α5β1 integrin bonds? We therefore measured the forces between Fn tips and α5β1 integrin-coated substrates (Figure S2). We found that the strength of the Fn−α5β1 integrin bond is 111 ± 7 nm (*n* = 266 adhesive force curves from five tips), consistent with values from live cell experiments (typically, ∼100 pN).[42,43] Periodic peaks separated by 31 ± 0.5 nm (*n* = 60) and typical of FnIII domain unfolding were frequently observed. Addition of RGD peptides led to a substantial reduction of binding probability, confirming the specificity of binding. These observations confirm the functionality of immobilized integrins.

There are two important outcomes of these analyses. First, the mechanical strength of the three-component FnBPA−Fn−integrin complex (∼800 pN) is much higher than that of single Fn−α5β1 integrin bonds (∼100 pN). This unusual mechanical response favors an activation model whereby, upon binding of Fn to FnBPA, mechanical forces will unfold FnIII domains, causing the exposure of buried integrin-binding sites, which in turn engages in a high-affinity interaction with integrin.[44] Second, the weak side of the three-component interaction is the Fn−integrin bond as the mechanical strength of the FnBPA−Fn β-zipper is very high (∼1500 pN). This could provide some cues for future therapeutic interventions against intracellular *S. aureus*.

Fn-Dependent Adhesion between *S. aureus* and Endothelial Cells. We wondered whether such Fn bridges occur between *S. aureus* and endothelial cells. To favor the exposure of α5β1 integrins in the upper cell membrane, endothelial cells were trypsinized to remove ECM proteins, immobilized on glass substrates coated with lectins, and then analyzed within less than 2 h.[43] Using this protocol, cells exposed large amounts of integrins on their upper membrane (Figure 5a,b). Force signatures detected after 1 s of interaction between Fn-saturated FnBPA[(+)] bacteria and endothelial cells showed several striking features (Figure 5c; data from three cell pairs; for more pairs, see Figure S3). Following maximum adhesion forces at short distances, F_{max} = 172 ± 57 pN (mean ± SD; *n* = 155 adhesive curves; Figure 5c), we observed discrete jumps resulting from the breakage of intermolecular bonds as well as constant force plateaus (see curves in the inset of Figure 5c) with a length up to 50 μm (Figure 5g). Extended force plateaus, which could only be captured using an unconventional extended *z*-range scanner (100 μm *vs* 15 μm), show that tethers were extracted from the cell membrane,[39,40] thus the bacteria had established direct contact with the cell membrane. *In vivo*, membrane tethers may help *S. aureus* bacteria to maintain adhesive contacts with host cells under mechanical stress. We also estimated the work of adhesion, W_{adh} = 0.5−6 fJ, by considering the area under the retraction curves (Figure S4 and Figure 5e).[40] As the bacterial cell wall is rigid and poorly deformable, the large W_{adh} value indicates that the soft, deformable cell membrane partly covers the bacterial cell surface, thus increasing the contact area and the adhesion energy. Overall, these observations point to the role of membrane deformation in determining the energy and duration of bacterial−host adhesion (Figure S4).

Several experiments support the notion that intercellular adhesion forces are associated with the Fn bridge between FnBPA and the α5β1 integrin. First, F_{max}, W_{adh}, and rupture length values were reduced when endothelial cells were incubated with anti-integrin antibodies or RGD peptides (Figure 6d−i), indicating that adhesion and tether formation involve the α5β1 integrin. Second, the same was also noted when using Fn-treated FnBPA[(−)] bacteria (Figure 6a−c), highlighting the role of FnBPA in the interaction. In summary,

we were able to quantify the forces driving the FnBPA−Fn−integrin interaction, both *in vitro* and on endothelial cells. The reason why the Fn bridge is mechanically weaker on endothelial cells is unclear, but this could result from the relatively weak anchoring strength of integrins in the membrane, as opposed to the strong covalent anchorage of immobilized integrins.

As FnBP-mediated internalization is a time-dependent process,[5] we finally looked into the dynamics of the Fn-dependent adhesion. Increasing the interaction time from 1 to 20 s led to higher F_{max} and W_{adh} values (Figure 5d,f,h), suggesting that, with time, the intercellular contact area increases and so does the overall adhesion. Following initial adhesion (<1 min), we hypothesized that pathogen−host interaction forces should further increase as internalization proceeds. To test this idea, single force curves were recorded on specific spots after 1 s, 1 min, 5 min, and 10 min. Here, a dramatic increase in adhesion was observed (W_{adh} = 1 ± 0.5 fJ at 1 s *vs* 51 ± 26 fJ at 10 min; Figure 7), demonstrating that, after the first minute, adhesion is strongly enhanced. We speculate that this time dependency involves two phenomena, that is, binding of multiple Fn molecules causing clustering of the integrins and subsequent intracellular signaling leading to endocytosis of the bacterial cell.

CONCLUSIONS

Invasion of mammalian cells by *S. aureus* involves Fn-dependent bridging between FnBPs on the bacterial surface and $\alpha5\beta1$ integrins in the host cell membrane, but the fundamental forces involved are poorly understood. We have used state of the art single-cell and single-molecule experiments to quantify the molecular forces engaged in this three-component interaction, revealing that the Fn bridge between FnBPA and the $\alpha5\beta1$ integrin is mechanically strong.

FnBPA promotes *S. aureus* adhesion to soluble Fn *via* molecular bonds that are very strong (~1500 pN). This high mechanical stability results from the cooperative loading of the multiple bonds of the tandem β-zipper formed between FnBPA and Fn. Weaker bonds are observed with fibrillar Fn, suggesting that detection of β-zipper structures depends on the anchoring strength and conformational state of the protein. Fn forms mechanically strong bridges between FnBPAs on the *S. aureus* cell surface and purified integrins that are capable of withstanding much higher forces (~800 pN) than the classical Fn−$\alpha5\beta1$ integrin interaction (~100 pN). This high mechanical stability favors an invasion model, whereby binding of Fn to FnBPA through a β-zipper leads to the force-induced unfolding and allosteric activation of FnIII domains. This results in the exposure of buried integrin-binding sites, which in turn engage in a strong, high-affinity interaction with integrins.[44] This activation mechanism emphasizes the importance of protein mechanobiology in bacterial−host adhesion. The mechanical strength of the Fn bridge is of biological relevance as it enables *S. aureus* to firmly attach to host cells and to efficiently trigger internalization, thereby helping the bacteria to evade host immune defenses and antibiotics. The interaction of *S. aureus* with host endothelial cells is also influenced by membrane deformation, which enhances the energy and duration of adhesion (Figure S4). Bacterial−host adhesion strengthens with time, an effect that may result from the clustering of integrins and from the internalization of the bacteria.

Our study shows promise for the identification of inhibitory compounds to treat infections involving intracellular pathogens.

Survival of *S. aureus* within host cells can not only help dissemination of the infection *via* the bloodstream[45] but also contribute to establish persistent infections through the formation of small colony variants[46,47] and persister cells.[48] Most antibiotics are not effective in killing intracellular bacteria due to their poor penetration into the host cell membrane. An appealing approach to overcome this problem is to develop inhibitors capable of interfering with the Fn bridge. We have shown that the Fn−integrin bond is the weak side of the three-component complex, as the Fn−FnBPA tandem β-zipper is mechanically very stable. This gives us some clues as how to target efficiently the Fn bridge for blocking invasion, that is, *via* the integrin side rather than the FnBPA side. Supporting this notion, we showed that antibodies and RGD peptides targeting the $\alpha5\beta1$ integrin strongly inhibit adhesion and invasion. These inhibitors could be used as therapeutic agents against intracellular *S. aureus*, as already suggested several years ago.[19] By blocking invasion, these agents could increase the efficacy of antibiotics which cannot efficiently pass through the cell membrane. So the combined use of inhibitory compounds and antibiotics could enhance antibiotic therapy. An alternative approach is to target the bacterial cell wall. Recently, a drug composed of a specific antibody targeting a surface component of *S. aureus* covalently linked to a potent antibiotic was shown to efficiently eradicate intracellular *S. aureus* infection, pointing to a promising strategy to kill *S. aureus* bacteria invading host tissues.[49] We speculate that AFM will contribute to the identification of compounds to efficiently inhibit cellular invasion by *S. aureus*.

While the main invasion pathway of *S. aureus* relies on FnBPs, other mechanisms are used by *S. aureus* to internalize host cells as mutants lacking FnBPs are often not completely deficient in invasion.[50] Such "back up" mechanisms are, for example, provided by the noncovalently cell-wall-bound autolysin Atl which can bind directly to the endothelial cell surface heat shock protein Hsc70.[51] Likewise, iron-regulated cell-wall-anchored protein IsdB promotes *S. aureus* adherence to and internalization by nonphagocytic human cells.[52] It has also been established that laminins that are primarily known for their function in the basement membrane act as a bridge between the host cells and several pathogens, including *S. aureus*, during bacterial invasion.[53] This suggests that laminin can function in a way that is reminiscent of the bridging function of Fn in FnBP-driven internalization of *S. aureus* into host cells.[53] These data indicate that *S. aureus* can invade host cells *via* multiple pathways. We anticipate that AFM will contribute to the identification of previously unknown *S. aureus* invasins and invasion mechanisms.

METHODS

Bacterial Strains and Growth Conditions. *S. aureus* strain FnBPA$^{(−)}$ (strain SH1000 *clfA clfB fnbA fnbB*) is defective in clumping factors A and B and fibronectin-binding proteins A and B.[54] FnBPA$^{(−)}$ cells were grown overnight in trypticase soy broth (TSB) at 37 °C with agitation, washed with TSB, and subcultured in exponential phase with a dilution of 1:100. Cells were allowed to grow to an optical density at 600 nm of 0.3−0.4 prior to harvesting of the cells. FnBPA$^{(+)}$ cells carrying the plasmid pFNBA4 expressing Fn-binding protein A from strain 8325-4[55] were cultured overnight in TSB and chloramphenicol (10 μg/mL) at 37 °C with agitation. Before experiments, cells were washed once in TSB and subcultured into TSB + chloramphenicol at 1:100 dilution until an OD$_{600}$ of 0.3−0.4 was reached. For harvesting, cells were centrifuged 3 min at 2000*g*, washed two times in phosphate buffer saline (PBS), and diluted 1:100

in PBS. For some experiments, bacteria were preincubated for 40 min with 0.05 mg mL^{-1} of soluble Fn, prepared as described below.

Cell Cultures. Human umbilical vein endothelial cells from a single donor (Lonza, Spain) were cultured in T25 flasks (Becton Dickinson, Germany), incubated at 37 °C, 5% CO$_2$, and 100% humidity. Commercial basal medium, supplemented with growth factors and cytokines (EGM BulletKit, Lonza), was used. For some experiments, cells from passages 3–9 were seeded on 35 mm Petri dishes 48 h prior to the experiment and were used after reaching confluence. In other experiments, cells were trypsinized and placed on 35 mm dishes, precoated with the concanavalin A (ConA) lectin (200 μg/mL, Sigma).

DNA Manipulation. DNA encoding FnBPA Fn-binding region (amino acids 512−872) was amplified by PCR using *S. aureus* 8325-4 genomic DNA as the template. Oligonucleotide primers were purchased from Integrated DNA Technologies (Leuven, Belgium). To amplify the Fn-binding region, primer FnBPA$_{512−872}$ forward (5′-AAGCACAAGGACCAGTCGAG-3′) and primer FnBPA$_{512−872}$ reverse (5′-TTATTGGTGTTTCCGGCTCACTT-3′) were used. Restriction enzyme cleavage sites *Bam*HI and *Eco*RI were incorporated at the 5′ ends of the primers to facilitate cloning into the pQE30 expression plasmid (Qiagen, Chatsworth, CA, USA). Restriction enzymes were purchased from New England BioLabs (Hertfordshire, United Kingdom). The integrity of cloned DNA was confirmed by sequencing (Primmbiotech, Milan, Italy).

Expression and Purification of Recombinant FnBPA Fn-Binding Region. Recombinant FnBPA fibronectin-binding region was expressed from pQE30 in *Escherichia coli* TOPP3 (Stratagene). Overnight starter cultures were diluted 1:50 in LB containing ampicillin (100 μg/mL) and incubated with shaking until the culture reached an optical density at 600 nm (OD600) of 0.4 to 0.6. Recombinant protein expression was induced by addition of isopropyl 1-thio-→-D-galactopyranoside (0.5 mM) and continued for 2 h. Bacterial cells were harvested by centrifugation and frozen at −80 °C. Recombinant protein was purified from cell lysates by Ni^{2+} affinity chromatography on a HiTrap chelating column (GE Healthcare, Buckinghamshire, United Kingdom). Protein purity was assessed to be 98% by SDS-PAGE, Coomassie brilliant blue staining, and densitometric analysis.

Purification of Plasma Fn. Human Fn was purified from plasma by a combination of gelatin- and arginine-sepharose affinity chromatography. The purity of the protein was assessed by 7.5% SDS-PAGE and Coomassie brilliant blue staining. To exclude the possibility of trace amounts of contaminants, affinity-purified Fn was spotted onto nitrocellulose membranes at different concentrations and overlaid with anti-Fn and antiplasminogen antibodies.[56]

Anti-Fn and Anti-integrin Antibodies. Mouse polyclonal antiserum against human Fn was generated by injecting BALB/c mice intraperitoneally five times at 1 week intervals with 50 μg of the purified antigen as reported.[57] The antibody was purified by affinity chromatography on protein A/sepharose according to the recommendations of the manufacturer (GE Healthcare). We also used commercially available mouse anti-α5β1 integrin antibody (MAB 1969, clone JBS5; Merck).

Adherence Assays. A crystal violet assay was also used to assess bacterial adhesion on Fn substrates. Microtiter wells were coated overnight at 4 °C with 1 μg/well human Fn in 0.1 M sodium carbonate (pH 9.5). The plates were washed with PBS containing 0.5% (v/v) Tween 20 (PBST). To block additional protein-binding sites, the wells were treated for 1 h at 22 °C with 2% (v/v) bovine serum albumin (BSA) in PBS. The wells were then incubated for 2 h at 37 °C with 1 × 10^8 *S. aureus* FnBPA$^{(−)}$ cells or *S. aureus* FnBPA$^{(+)}$ cells. After being washed with PBS, adhering cells were fixed with 2.5% formaldehyde for 30 min and stained with 1% crystal violet for 1 min. After being washed, 100 μL of 10% acetic acid was added, and absorbance at 595 nm was recorded using an ELISA plate reader (BioRad, CA).

Endothelial Cell Invasion Assay. HUVEC were cultured in endothelial basal medium (EBM) supplemented with 2% fetal bovine serum (FBS), 0.4% bovine brain extract, 0.1% human epidermal growth factor, 0.1% hydrocortisone, 0.1% ascorbic acid, and 0.1% gentamicin/amphotericin at 37 °C in 5% CO$_2$ according to manufacturer's instructions (Lonza). Cultured cells were dissociated from plastic flasks using trypsin-EDTA solution (Lonza) and approximately 5 × 10^5 cells (in 1 mL of EBM medium without antibiotics) were seeded into 24-well plates (Nunc) and allowed to attach for 48 h at 37° in 5% CO$_2$. Cell confluence was verified with an inverted light microscope. Each well was washed once in PBS and incubated with 1 × 10^7 bacterial cells in EMB medium containing 10% FBS without antibiotics for 90 min at 37 °C in 5% CO$_2$. Then, the culture supernatants were removed from the wells and replaced with 500 μL of EMB medium supplemented with 200 μg/mL gentamicin. The wells were further incubated for 90 min at 37 °C in 5% CO$_2$. After several washings with PBS, the wells were added with 500 μL of 0.5% Triton X-100 in PBS for 10 min at 37 °C in 5% CO$_2$. To ensure the cells fully lyse and release all the internalized bacteria, the suspensions were agitated by pipetting, and CFU were quantified by serial dilution and plating onto TSB agar plates incubated overnight at 37 °C.

Immunofluorescence Microscopy. To image Fn in the extracellular matrix, confluent cell monolayers on glass were fixed with 4% paraformaldehyde in PBS for 10 min without further permeabilization, pretreated with 10% bovine serum albumin at room temperature for 30 min, and incubated up to 120 min at room temperature with anti-Fn antibodies. A secondary goat anti-mouse Alexa Fluor 488 antibody (Abcam) was added for 60 min after washing with PBS. For visualization of α5β1 integrins, cells attached on glass or ConA surfaces were fixed with 4% paraformaldehyde in PBS for 10 min and permeabilized at room temperature with 0.1% Triton X-100 (Sigma-Aldrich) for 1 min. To prevent nonspecific antibody binding, endothelial cells were pretreated with 10% BSA (Sigma) at room temperature for 30 min and then incubated up to 120 min at room temperature with anti-α5β1 integrin antibody. After being washed with PBS, a secondary goat anti-mouse Alexa Fluor 647 antibody (Abcam) was added for 60 min. All samples were stained with DAPI to facilitate the identification of the correct focal plane. Finally, coverslips were mounted in mounting medium (DAKO, Germany). Fluorescent images were acquired using a Zeiss LSM 710 confocal laser scanning microscope, equipped with an 63× NA 1.4 HC PL APO CS2 oil immersion objective. The fluorophores were excited at 488, 561, or 405 nm. Sequential scanning was applied to avoid concurrent fluorescence signals from two fluorophores.

For imaging bacterial invasion, confluent HUVEC cultured for at least 48 h were co-incubated with *S. aureus* bacterial cells in the exponential phase (50 μL of a diluted cell suspension per 1 mL of medium) up to 40 min at room temperature and then fixed with 4% paraformaldehyde in PBS for 10 min. To visualize α5β1 integrins on host cells, samples were pretreated with 10% BSA for 30 min and then incubated 60 min at room temperature with mouse anti-α5β1 integrin antibody (MAB 1969; clone JBS5; Merck). After being washed with PBS, a secondary goat anti-mouse Alexa Fluor 647 antibody (Abcam) was added for 60 min. Moreover, samples were stained with DAPI for identification of host cells nucleous and bacterial cells. Coverslips were mounted in mounting medium (DAKO, Germany). We performed three-dimensional image analysis using a Zeiss LSM 710 confocal laser scanning microscope equipped with an 63× NA1.4 HC PL APO CS2 oil immersion objective. Fluorophores were excited at 561 and 405 nm, and vertical and horizontal cross sections of the infected host cells confirmed the internalization of bacteria.

Fn and Integrin-Coated Substrates. Fn (see above) and recombinant human integrin α5β1 (R&D Systems, Minneapolis) were attached to gold-coated surfaces *via* N-hydroxysuccinimide (NHS) surface chemistry. To this end, gold-coated glass substrates were immersed overnight in ethanol solutions containing 1 mM 16-mercaptohexadecanoic acid (Sigma) and 11-mercapto-1-undecanol (Sigma) at a molar ratio of 10:90 and were then rinsed with ethanol. Substrates were immersed for 30 min in a solution containing 10 mg mL^{-1} NHS (Sigma) and 25 mg mL^{-1} 1-ethyl-3-(3-(dimethylamino)-propyl)-carbodiimide (EDC) (Sigma), rinsed, and then incubated with PBS containing 0.2 mg mL^{-1} Fn or 0.1 mg mL^{-1} integrins for 1 h, followed by rinsing with PBS.

Single-Molecule Force Spectroscopy on Model Surfaces and on Living Bacteria. AFM tips were functionalized with Fn or with recombinant Fn-binding repeats from FnBPA (see above). Proteins were attached to gold-coated cantilevers (Olympus OTR4, $k \sim 0.02$ N m^{-1}) via NHS surface chemistry. Cantilevers were immersed overnight in ethanol solutions containing 1 mM 16-mercaptohexadecanoic acid (Sigma) and 11-mercapto-1-undecanol (Sigma) at a molar ratio of 1:90 and were then rinsed with ethanol. They were immersed for 30 min in a solution containing 10 mg mL^{-1} NHS (Sigma) and 25 mg mL^{-1} EDC (Sigma), rinsed, and then incubated with PBS containing 0.2 mg mL^{-1} of Fn or FnBPA fragments for 1 h, followed by rinsing with PBS.

For bacterial cell analysis, bacteria were immobilized by mechanical trapping into porous polycarbonate membranes (Millipore, Billerica, MA) with a pore size similar to the cell size. After filtration of a cell suspension was performed, the filter was gently rinsed with PBS, carefully cut into sections (1 cm by 1 cm), and attached to a steel sample puck using a small piece of double-sided adhesive tape, and the mounted sample was transferred into the AFM liquid cell while avoiding dewetting.

SMFS analyses were performed with live cells at room temperature (20 °C) in HEPES buffer (HEPES, 10 mM; glucose, 5 mM; MgCl$_2$, 1 mM; KCl, 5 mM; NaCl, 140 mM; pH 7.4) using a Nanoscope VIII multimode AFM (Bruker Corporation, Santa Barbara, CA) and gold-coated cantilevers (Olympus OTR4, $k \sim 0.02$ N m^{-1}). All curves were obtained using a contact time of 100 ms, a maximum applied force of 250 pN, and approach and retraction speeds of 1000 nm·s^{-1}. The spring constants of the cantilevers were measured using the thermal noise method.

Single-Cell Force Spectroscopy on Model Surfaces. Colloidal probes were prepared by attaching single silica microsphere (6.1 μm diameter, Bangs Laboratories) with a thin layer of UV-curable glue (NOA 63, Norland Edmund Optics) on triangular shaped tipless cantilevers (NP-O10, Bruker) and using a Nanoscope VIII (Bruker Corporation, Santa Barbara, CA). Cantilevers were then immersed for 1 h in a 10 mM Tris buffer + 150 mM NaCl solution (pH 8.5) containing 4 mg/mL dopamine hydrochloride (99%, Sigma), rinsed in Tris buffer + 150 mM NaCl solution (pH 8.5), and used directly for cell probe preparation. The nominal spring constant of the colloidal probe cantilever was determined by the thermal noise method. For cell probe preparation, 50 μL of a cell suspension was transferred into a glass Petri dish containing Fn-coated of integrin-coated substrates in HEPES buffer. The colloidal probe was brought into contact with a bacterium. Single bacteria were attached on the center of the colloidal probes using a Bioscope Catalyst AFM (Bruker, Santa Barbara, CA) equipped with a Zeiss Axio observer Z1 stand and a Hamamatsu camera (model C10600). The cell probe was then positioned over the Fn or integrin substrates without dewetting. Multiple force curves were recorded at room temperature (20 °C) on five different spots, using a Bioscope Catalyst AFM (Bruker, Santa Barbara, CA). All curves were obtained using a contact time of 100 ms, a maximum applied force of 250 pN, and approach and retraction speeds of 1000 nm·s^{-1}.

Single-Cell Force Spectroscopy on Endothelial Cells. Colloidal probes were obtained as described above using tipless cantilevers (NP-O10, Bruker) and a Nanowizard III AFM (JPK Instrument, Berlin, Germany). They were immersed for 1 h in Tris-buffered saline (TBS; Tris, 10 mM; NaCl, 150 mM; pH 8.5) containing 4 mg·mL^{-1} dopamine hydrochloride (Sigma-Aldrich), rinsed in TBS, and used directly for cell probe preparation. The nominal spring constant of the colloidal probe was determined by the thermal noise method. Then, 50 μL of a diluted cell suspension was deposited into the Petri dish containing HUVEC at a distinct location within the Petri dish; 3 mL of HEPES buffer was added to the system. The colloidal probe was put in contact with a single bacterial cell and retracted to attach it on the silica microsphere; proper attachment of the cell on the colloidal probe was checked using optical microscopy. The obtained cell probe was then transferred over a HUVEC. Force measurements were performed at room temperature (20 °C) in medium using a Nanowizard III AFM, using either the standard configuration or the CellHesion module (JPK Instruments). Multiple

force–distance curves (8×8 or 32×32) were recorded across 1 μm $\times$ 1 μm areas of HUVEC, using an applied force of 250 pN, a constant approach–retraction speed of 1.0 μm·s^{-1} (for the standard system) or 5.0 μm·s^{-1} (for CellHesion AFM module). For some blocking experiments, we used the commercially available RGDFV peptide (Sigma-Aldrich). Data were analyzed using the data processing software from JPK Instruments (Berlin, Germany).

ASSOCIATED CONTENT

ⓢ Supporting Information

The Supporting Information is available free of charge on the ACS Publications website at DOI: 10.1021/acsnano.8b00716.

Figures S1−S4 (PDF)

AUTHOR INFORMATION

Corresponding Authors
*E-mail: pspeziale@unipv.it.
*E-mail: yves.dufrene@uclouvain.be.

ORCID
David Alsteens: 0000-0001-9229-113X
Giampiero Pietrocola: 0000-0002-7069-8155

Author Contributions
V.P., C.F., and P.H. contributed equally. V.P., C.F., P.H.B., F.V.B., D.A., G.P., P.S., and Y.F.D. designed the experiments, analyzed the data, and wrote the article. V.P., C.F., P.H.B., F.V.B., and G.P. collected the data.

Notes
The authors declare no competing financial interest.

REFERENCES

(1) Ogawa, S. K.; Yurberg, E. R.; Hatcher, V. B.; Levitt, M. A.; Lowy, F. D. Bacterial Adherence to Human Endothelial Cells *in vitro*. *Infect. Immun.* **1985**, *50*, 218–224.
(2) Menzies, B. E.; Kourteva, I. Internalization of *Staphylococcus aureus* by Endothelial Cells Induces Apoptosis. *Infect. Immun.* **1998**, *66*, 5994–5998.
(3) Bayles, K. W.; Kenneth, W.; Wesson, C. A.; Liou, L. E.; Fox, L. K.; Bohach, G. A.; Trumble, W. R. Intracellular *Staphylococcus aureus* Escapes the Endosome and Induces Apoptosis in Epithelial Cells. *Infect. Immun.* **1998**, *66*, 336–342.
(4) Dziewanowska, K.; Patti, J. M.; Deobald, C. F.; Bayles, K. W.; Trumble, W. R.; Bohach, G. A. Fibronectin Binding Protein and Host Cell Tyrosine Kinase are Required for Internalization of *Staphylococcus aureus* by Epithelial Cells. *Infect. Immun.* **1999**, *67*, 4673–4678.
(5) Sinha, B.; Francois, P. P.; Nüße, O.; Foti, M.; Hartford, O. M.; Vaudaux, P.; Foster, T. J.; Lew, D. P.; Herrmann, M.; Krause, K. H. Fibronectin-binding Protein Acts as *Staphylococcus aureus* Invasin via Fibronectin Bridging to Integrin $\alpha5\beta1$. *Cell. Microbiol.* **1999**, *1*, 101–117.

(6) Ellington, J. K.; Reilly, S. S.; Ramp, W. K.; Smeltzer, M. S.; Kellam, J. F.; Hudson, M. C. Mechanisms of *Staphylococcus aureus* Invasion of Cultured Osteoblasts. *Microb. Pathog.* **1999**, *26*, 317−323.

(7) Jevon, M.; Guo, C.; Ma, B.; Mordan, N.; Nair, S. P.; Harris, M.; Henderson, B.; Bentley, G.; Meghji, S. Mechanisms of Internalization of *Staphylococcus aureus* by Cultured Human Osteoblasts. *Infect. Immun.* **1999**, *67*, 2677−2681.

(8) Foster, T. J.; Geoghegan, J. A.; Ganesh, V. K.; Höök, M. Adhesion, Invasion and Evasion: the Many Functions of the Surface Proteins of *Staphylococcus aureus*. *Nat. Rev. Microbiol.* **2014**, *12*, 49−62.

(9) Edwards, A. M.; Bowden, M. G.; Brown, E. L.; Laabei, M.; Massey, R. C. *Staphylococcus aureus* Extracellular Adherence Protein Triggers TNFα Release, Promoting Attachment to Endothelial Cells *via* Protein A. *PLoS One* **2012**, *7*, e43046.

(10) Claes, J.; Vanassche, T.; Peetermans, M.; Liesenborghs, L.; Vandenbriele, C.; Vanhoorelbeke, K.; Missiakas, D.; Schneewind, O.; Hoylaerts, M. F.; Heying, R.; Verhamme, P. Adhesion of *Staphylococcus aureus* to the Vessel Wall Under Flow is Mediated by von Willebrand Factor−binding Protein. *Blood* **2014**, *124*, 1669−1676.

(11) McDonnell, C. J.; Garciarena, C. D.; Watkin, R. L.; McHale, T. M.; McLoughlin, A.; Claes, J.; Verhamme, P.; Cummins, P. M.; Kerrigan, S. W. Inhibition of Major Integrin αVβ3 Reduces *Staphylococcus aureus* Attachment to Sheared Human Endothelial Cells. *J. Thromb. Haemostasis* **2016**, *14*, 2536−2547.

(12) Sinha, B.; Herrmann, M. Mechanism and Consequences of Invasion of Endothelial Cells by *Staphylococcus aureus*. *Thromb. Haemostasis* **2005**, *94*, 266−277.

(13) Massey, R. C.; Kantzanou, M. N.; Fowler, T.; Day, N. P.; Schofield, K.; Wann, E. R.; Berendt, A. R.; Höök, M.; Peacock, S. J. Fibronectin-binding Protein A of *Staphylococcus aureus* has Multiple, Substituting, Binding Regions that Mediate Adherence to Fibronectin and Invasion of Endothelial Cells. *Cell. Microbiol.* **2001**, *3*, 839−851.

(14) Edwards, A. M.; Potts, J. R.; Josefsson, E.; Massey, R. C. *Staphylococcus aureus* Host Cell Invasion and Virulence in Sepsis is Facilitated by the Multiple Repeats within FnBPA. *PLoS Pathog.* **2010**, *6*, e1000964.

(15) Schwarz-Linek, U.; Werner, J. M.; Pickford, A. R.; Gurusiddappa, S.; Kim, J. H.; Pilka, E. S.; Briggs, J. A.; Gough, T. S.; Höök, M.; Campbell, I. D.; Potts, J. R. Pathogenic Bacteria Attach to Human Fibronectin Through a Tandem β-zipper. *Nature* **2003**, *423*, 177−181.

(16) Meenan, N. A.; Visai, L.; Valtulina, V.; Schwarz-Linek, U.; Norris, N. C.; Gurusiddappa, S.; Höök, M.; Speziale, P.; Potts, J. R. The Tandem β-zipper Model Defines High Affinity Fibronectin-binding Repeats within *Staphylococcus aureus* FnBPA. *J. Biol. Chem.* **2007**, *282*, 25893−25902.

(17) Dufrêne, Y. F. Sticky Microbes: Forces in Microbial Cell Adhesion. *Trends Microbiol.* **2015**, *23*, 376−382.

(18) Xiao, J.; Dufrêne, Y. F. Optical and Force Nanoscopy in Microbiology. *Nat. Microbiol.* **2016**, *1*, 16186.

(19) Pierschbacher, M. D.; Ruoslahti, E. Cell Attachment Activity of Fibronectin can be Duplicated by Small Synthetic Fragments of the Molecule. *Nature* **1984**, *309*, 30−33.

(20) Ruoslahti, E. RGD and Other Recognition Sequences for Integrins. *Annu. Rev. Cell Dev. Biol.* **1996**, *12*, 697−715.

(21) Fowler, T.; Wann, E. R.; Joh, D.; Johansson, S.; Foster, T. J.; Höök, M. Cellular Invasion by *Staphylococcus aureus* Involves a Fibronectin Bridge Between the Bacterial Fibronectin-Binding MSCRAMMs and Host Cell β1 Integrins. *Eur. J. Cell Biol.* **2000**, *79*, 672−679.

(22) Lower, S. K.; Lamlertthon, S.; Casillas-Ituarte, N. N.; Lins, R. D.; Yongsunthon, R.; Taylor, E. S.; DiBartola, A. C.; Edmonson, C.; McIntyre, L. M.; Reller, L. B.; Que, Y. A.; et al. Polymorphisms in Fibronectin Binding Protein A of *Staphylococcus aureus* are Associated with Infection of Cardiovascular Devices. *Proc. Natl. Acad. Sci. U. S. A.* **2011**, *108*, 18372−18377.

(23) Matthews, J. M.; Potts, J. R. The Tandem β-zipper: Modular Binding of Tandem Domains and Linear Motifs. *FEBS Lett.* **2013**, *587*, 1164−1171.

(24) Bustanji, Y.; Arciola, C. R.; Conti, M.; Mandello, E.; Montanaro, L.; Samorí, B. Dynamics of the Interaction Between a Fibronectin Molecule and a Living Bacterium under Mechanical Force. *Proc. Natl. Acad. Sci. U. S. A.* **2003**, *100*, 13292−13297.

(25) Xu, C. P.; Boks, N. P.; de Vries, J.; Kaper, H. J.; Norde, W.; Busscher, H. J.; van der Mei, H. C. *Staphylococcus aureus*-fibronectin Interactions with and without Fibronectin-binding Proteins and their Role in Adhesion and Desorption. *Appl. Environ. Microbiol.* **2008**, *74*, 7522−7528.

(26) Lower, S. K.; Yongsunthon, R.; Casillas-Ituarte, N. N.; Taylor, E. S.; DiBartola, A. C.; Lower, B. H.; Beveridge, T. J.; Buck, A. W.; Fowler, V. G. A Tactile Response in *Staphylococcus aureus*. *Biophys. J.* **2010**, *99*, 2803−2811.

(27) Buck, A. W.; Fowler, V. G., Jr; Yongsunthon, R.; Liu, J.; DiBartola, A. C.; Que, Y. A.; Moreillon, P.; Lower, S. K. Bonds Between Fibronectin and Fibronectin-binding Proteins on *Staphylococcus aureus* and *Lactococcus lactis*. *Langmuir* **2010**, *26*, 10764−10770.

(28) Casillas-Ituarte, N. N.; Lower, B. H.; Lamlertthon, S.; Fowler, V. G.; Lower, S. K. Dissociation Rate Constants of Human Fibronectin Binding to Fibronectin-binding Proteins on Living *Staphylococcus aureus* Isolated from Clinical Patients. *J. Biol. Chem.* **2012**, *287*, 6693−6701.

(29) Casillas-Ituarte, N. N.; Cruz, C. H.; Lins, R. D.; DiBartola, A. C.; Howard, J.; Liang, X.; Höök, M.; Viana, I. F.; Sierra-Hernández, M. R.; Lower, S. K. Amino Acid Polymorphisms in the Fibronectin-binding Repeats of Fibronectin-binding Protein A Affect Bond Strength and Fibronectin Conformation. *J. Biol. Chem.* **2017**, *292*, 8797−8810.

(30) Beaussart, A.; El-Kirat-Chatel, S.; Herman, P.; Alsteens, D.; Mahillon, J.; Hols, P.; Dufrêne, Y. F. Single-Cell Force Spectroscopy of Probiotic Bacteria. *Biophys. J.* **2013**, *104*, 1886−1892.

(31) Beaussart, A.; El-Kirat-Chatel, S.; Sullan, R. M. A.; Alsteens, D.; Herman, P.; Derclaye, S.; Dufrêne, Y. F. Quantifying the Forces Guiding Microbial Cell Adhesion Using Single-Cell Force Spectroscopy. *Nat. Protoc.* **2014**, *9*, 1049−1055.

(32) Grandbois, M.; Beyer, M.; Rief, M.; Clausen-Schaumann, H.; Gaub, H. E. How Strong is a Covalent Bond? *Science* **1999**, *283*, 1727−1730.

(33) Kellermayer, M. S.; Grama, L.; Karsai, Á.; Nagy, A.; Kahn, A.; Datki, Z. L.; Penke, B. Reversible Mechanical Unzipping of Amyloid β-fibrils. *J. Biol. Chem.* **2005**, *280*, 8464−8470.

(34) Alsteens, D.; Ramsook, C. B.; Lipke, P. N.; Dufrêne, Y. F. Unzipping a Functional Microbial Amyloid. *ACS Nano* **2012**, *6*, 7703−7711.

(35) Rief, M.; Clausen-Schaumann, H.; Gaub, H. E. Sequence-dependent Mechanics of Single DNA Molecules. *Nat. Struct. Biol.* **1999**, *6*, 346−349.

(36) Herman-Bausier, P.; El-Kirat-Chatel, S.; Foster, T. J.; Geoghegan, J. A.; Dufrêne, Y. F. *Staphylococcus aureus* Fibronectin-binding Protein A Mediates Cell-cell Adhesion Through Low-affinity Homophilic Bonds. *mBio* **2015**, *6*, e00413-15.

(37) Vakonakis, I.; Campbell, I. D. Extracellular Matrix: from Atomic Resolution to Ultrastructure. *Curr. Opin. Cell Biol.* **2007**, *19*, 578−583.

(38) Singh, P.; Carraher, C.; Schwarzbauer, J. E. Assembly of Fibronectin Extracellular Matrix. *Annu. Rev. Cell Dev. Biol.* **2010**, *26*, 397−419.

(39) Evans, E. A.; Calderwood, D. A. Forces and Bond Dynamics in Cell Adhesion. *Science* **2007**, *316*, 1148−1153.

(40) Helenius, J.; Heisenberg, C. P.; Gaub, H. E.; Muller, D. J. Single-cell Force Spectroscopy. *J. Cell Sci.* **2008**, *121*, 1785−1791.

(41) Oberhauser, A. F.; Badilla-Fernandez, C.; Carrion-Vazquez, M.; Fernandez, J. M. The Mechanical Hierarchies of Fibronectin Observed with Single-molecule AFM. *J. Mol. Biol.* **2002**, *319*, 433−447.

(42) Li, F.; Redick, S. D.; Erickson, H. P.; Moy, V. T. Force Measurements of the α5β1 Integrin−Fibronectin Interaction. *Biophys. J.* **2003**, *84*, 1252−1262.

(43) Bharadwaj, M.; Strohmeyer, N.; Colo, G. P.; Helenius, J.; Beerenwinkel, N.; Schiller, H. B.; Fässler, R.; Müller, D. J. αV-class

Integrins Exert Dual Roles on $\alpha5\beta1$ Integrins to Strengthen Adhesion to Fibronectin. *Nat. Commun.* **2017**, *8*, 14348.

(44) Liang, X.; Garcia, B. L.; Visai, L.; Prabhakaran, S.; Meenan, N. A.; Potts, J. R.; Humphries, M. J.; Höök, M. Allosteric Regulation of Fibronectin/$\alpha5\beta1$ Interaction by Fibronectin-binding MSCRAMMs. *PLoS One* **2016**, *11*, e0159118.

(45) Horn, J.; Stelzner, K.; Rudel, T.; Fraunholz, M. Inside job: *Staphylococcus aureus* Host-Pathogen Interactions. *Int. J. Med. Microbiol.* **2017**, DOI: 10.1016/j.ijmm.2017.11.009.

(46) Vesga, O.; Groeschel, M. C.; Otten, M. F.; Brar, D. W.; Vann, J. M.; Proctor, R. A. *Staphylococcus aureus* Small Colony Variants are Induced by the Endothelial Cell Intracellular Milieu. *J. Infect. Dis.* **1996**, *173*, 739−742.

(47) Löffler, B.; Tuchscherr, L.; Niemann, S.; Peters, G. *Staphylococcus aureus* Persistence in Non-professional Phagocytes. *Int. J. Med. Microbiol.* **2014**, *304*, 170−176.

(48) Maisonneuve, E.; Gerdes, K. Molecular Mechanisms Underlying Bacterial Persisters. *Cell* **2014**, *157*, 539−548.

(49) Lehar, S. M.; Pillow, T.; Xu, M.; Staben, L.; Kajihara, K. K.; Vandlen, R.; DePalatis, L.; Raab, H.; Hazenbos, W. L.; Morisaki, J. H.; Kim, J.; et al. Novel Antibody−antibiotic Conjugate Eliminates Intracellular *S. aureus*. *Nature* **2015**, *527*, 323−328.

(50) Diot, A.; Laurent, F.; Josse, J. Staphylococcal Adhesion and Host Cell Invasion: Fibronectin-binding and Other Mechanisms. *Front. Microbiol.* **2017**, *8*, 2433.

(51) Hirschhausen, N.; Schlesier, T.; Schmidt, M. A.; Götz, F.; Peters, G.; Heilmann, C. A. Novel Staphylococcal Internalization Mechanism Involves the Major Autolysin Atl andHheat Shock Cognate Protein Hsc70 as Host Cell Receptor. *Cell. Microbiol.* **2010**, *12*, 1746−1764.

(52) Zapotoczna, M.; Jevnikar, Z.; Miajlovic, H.; Kos, J.; Foster, T. J. Iron-regulated Surface Determinant B (IsdB) Promotes *Staphylococcus aureus* Adherence to and Internalization by Non-phagocytic Human Cells. *Cell. Microbiol.* **2013**, *15*, 1026−1041.

(53) van Wijk, X. M.; Döhrmann, S.; Hallström, B. M.; Li, S.; Voldborg, B. G.; Meng, B. X.; McKee, K. K.; van Kuppevelt, T. H.; Yurchenco, P. D.; Palsson, B. O.; Lewis, N. E.; et al. Whole-genome Sequencing of Invasion-resistant Cells Identifies Laminin $\alpha2$ as a Host Factor for Bacterial Invasion. *mBio* **2017**, *8*, e02128-16.

(54) O'Neill, E.; Pozzi, C.; Houston, P.; Humphreys, H.; Robinson, D. A.; Loughman, A.; Foster, T. J.; O'Gara, J. P. A Novel *Staphylococcus aureus* Biofilm Phenotype Mediated by the Fibronectin-binding Proteins, FnBPA and FnBPB. *J. Bacteriol.* **2008**, *190*, 3835−3850.

(55) Geoghegan, J. A.; Monk, I. R.; O'Gara, J. P.; Foster, T. J. Subdomains N2N3 of Fibronectin Binding Protein A Mediate *Staphylococcus aureus* Biofilm Formation and Adherence to Fibrinogen Using Distinct Mechanisms. *J. Bacteriol.* **2013**, *195*, 2675−2683.

(56) Speziale, P.; Visai, L.; Rindi, S.; Di Poto, A. Purification of Human Plasma Fibronectin Using Immobilized Gelatin and Arg Affinity Chromatography. *Nat. Protoc.* **2008**, *3*, 525−533.

(57) Pietrocola, G.; Geoghegan, J. A.; Rindi, S.; Di Poto, A.; Missineo, A.; Consalvi, V.; Foster, T. J.; Speziale, P. Molecular Characterization of the Multiple Interactions of SpsD, a Surface Protein from *Staphylococcus pseudintermedius*, with Host Extracellular Matrix Proteins. *PLoS One* **2013**, *8*, e66901.